Conference Proceedings

EuroSun 2016
Palma de Mallorca (Spain), 11 - 14 October 2016

# Performance Evaluation and Trial Making of a Compact Solar EV

**Toru Fujisawa[1] and Takashi Kawaguchi[1]**

[1] Kanagawa Institute of Technology, Atsugi (Japan)

## Abstract

In this study, we built a compact solar electric vehicle (EV) converted from a Honda Gyro Canopy, which is a three wheel scooter widely used in Japan for delivery services, and installed bifacial c-Si PV modules on the surface of its delivery box. The power generated from the photovoltaic (PV) modules was controlled using a quad peak power tracker (PPT) system in the solar EV. In this paper, we discuss three types of PPT systems that can maximize the charging power from PV modules to the four valve-regulated lead-acid storage batteries. Moreover, we evaluated the energetic performance of the solar EV running on a Li-ion storage battery of 5 kg. The outdoor experiments clearly showed that four series–parallel PPT systems produce better electrical energy than the other systems. The average energy consumption by the solar EV circling a building on a flat asphalt pavement road was 1.06 kW at an average speed of 15.9 km/h (peak speed was 25.1 km/h).

Keywords: *Solar EV, EV conversion, PV system, bifacial c-Si, multiple peak power tracker.*

## 1. Introduction

In 2015, the number of Honda Gyro (GYRO) Canopy vehicles manufactured in Japan was over 240,000 (Honda Gyro, 2015). The GYRO is a three-wheel scooter, popular for delivery services in Japan, and has an engine displacement of under 50 cc.

Fig. 1 shows a solar electric vehicle (EV) converted from the GYRO Canopy with bifacial c-Si photovoltaic (PV) modules on its delivery box. The powertrain of the solar EV is a surface-mounted permanent magnet synchronous motor (SPMSM; outer rotor type, with 12 poles, 18 teeth, and 6 coils in parallel with a Y connection, as indicated in Table 1), as shown in Fig. 2. Its reduction gear ratio was 29.86 after the conversion.

**Fig. 1: Solar EV (EV conversion of HONDA GYRO CANOPY)**

**Fig. 2: SPMSM**


doi:10.18086/eurosun.2016.08.05 Available at http://proceedings.ises.org

**Tab. 1: Specification of the blushless DC motor.**

| Item | Value |
|---|---|
| Core diameter | 94.7 mm |
| Core thickness | 27.0 mm |
| Air gap | 0.85 mm |
| Permanent magnet | FB6B (Br = 420 mT) |
| Slot／Pole | 18／12 |
| Turns of 1 slot | 25 turns |
| Wire type | Polyester enamel wire |
| Wire diameter | 1.0 mm |
| Winding and Connection | 3 phase 6 parallel, Y connection |

## 2. PV system

### *2.1. PV cell and PV module*

Fig. 3 shows the unit cell of bifacial c-Si PV produced by bSolar (2012) comprising a cut cell, laminated cell layout, and weight of the module. The laminated modules are installed on four surfaces (top, back, left, and right) of the delivery box. Table 2 lists the ratings as typical values of bifacial c-Si PV module under the standard test condition (STC) of 1kW/m$^2$, A.M.1.5, and 25 °C.

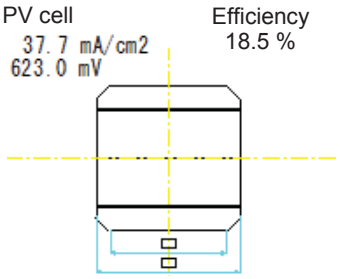


**(a) 156 × 156 mm cell**

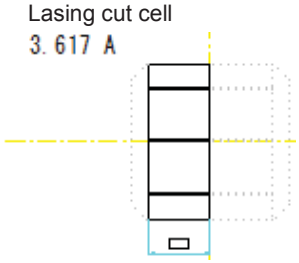


**(b) 156 × 61.5 mm cut cell**

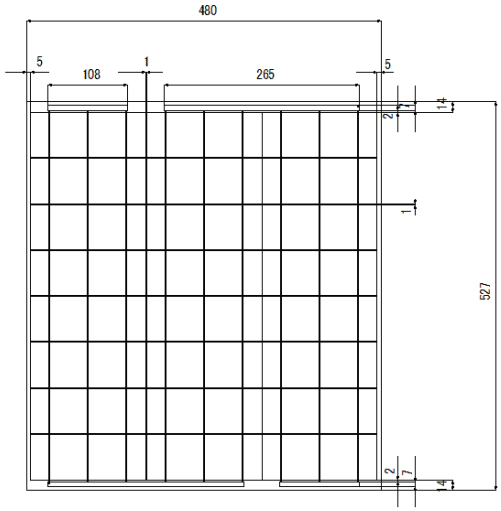


**(c) Laminated PV module made from the cut cell (24 cell types)**

**(d) Weight of laminated module (approx. 0.5 kg for a 24-cell module)**

**Fig. 3: Laminated PV module of bifacial c-Si**

**Tab. 2: Ratings of bifacial c-Si PV module (Typical value for 24 cells)**

| surface | Voc [V] | Isc [A] | Vmax [V] | Imax [A] | Pmax [W] | FF [ - ] |
|---|---|---|---|---|---|---|
| **Primary** | 14.50 | 3.52 | 11.74 | 3.31 | 38.87 | 0.76 |
| **Secondary** | 14.36 | 2.82 | 11.77 | 2.67 | 31.41 | 0.78 |

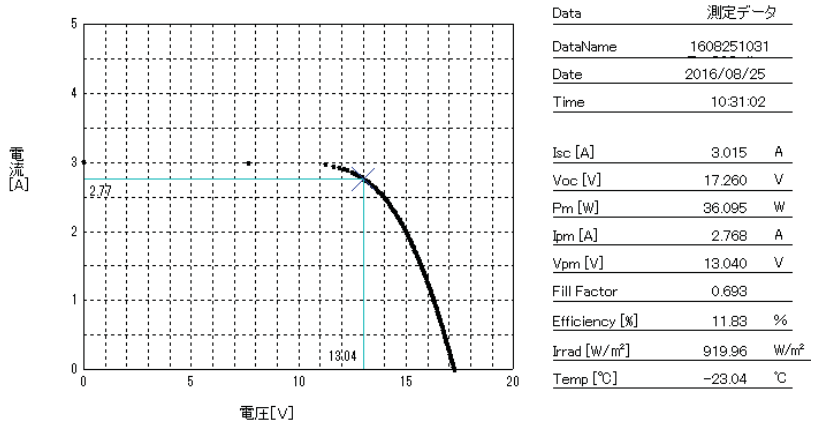


**Fig. 4: I–V characteristic curve of the top 32 cells obtained from outdoor experiments (25th AUG, 2016; 10:31)**

Fig. 4 illustrates the I–V characteristic curve of the 32-cells PV module on the top surface of the delivery box. A temperature sensor was not connected, and the PV module is second hand. However, a smooth curve and a peak power current of 2.8 A were obtained in outdoor (with reduced irradiance and increased temperature).

### *2.2. PV system (Peak Power Tracker)*

On the delivery box, PV modules on the top surface consist of 32 cells, and the other three vertical surfaces (back, left, and right surfaces) have 24 cells each. We used four boost dc–dc type peak power trackers (PPTs; of one-chip and an efficiency of up to 98%, as developed by STMicroelectronics, 2012) for those PV modules (Fig. 5). A distributed PPT in stationary PV array, evaluation and introduction has discussed by Youhei et al. (2013). Takanori et al. demonstrated a distributed PPT on a racing solar car (2014). To evaluate a multiple PPT system, we tested three connections (Fig. 6). In addition, a series PPT system and series–parallel PPT system were compared through outdoor experiments at the north parking (as shown in Fig. 6). The series–parallel system consists of a pair of parallel PPTs in series with other PPTs; this arrangement is aimed at recovering lower power of the PV module by adding current to the left, right, back, and top of the delivery box.

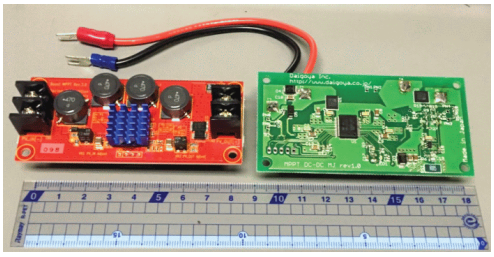

**Fig. 5: Boost-type peak power tracker (SPV1020)**

## 3. Outdoor experiments

### *3.1. Trial experiment of PV power generation*

Fig. 7 and Table 3 show some results of outdoor experiments of the series and series–parallel PPT systems. For these experiments, the solar EV was tested at the north parking with the PV module of its back side facing the south; the measuring period was 10:30–15:30 (logging data by every 10 s). As indicated in Fig. 7 and Table 3, every output power was kept low in the trial experiments because few protection settings in the PPT circuit board, such as the input voltage, output current, and output voltage, were not suitable. Thus, the PV module's current was limited to less than 0.3 A based on the PPT settings. However, every PPT system can function for

different surfaces and irradiance conditions. In Table 3 and Fig. 7, the measured powers are normalized based on the top surface's PV module.

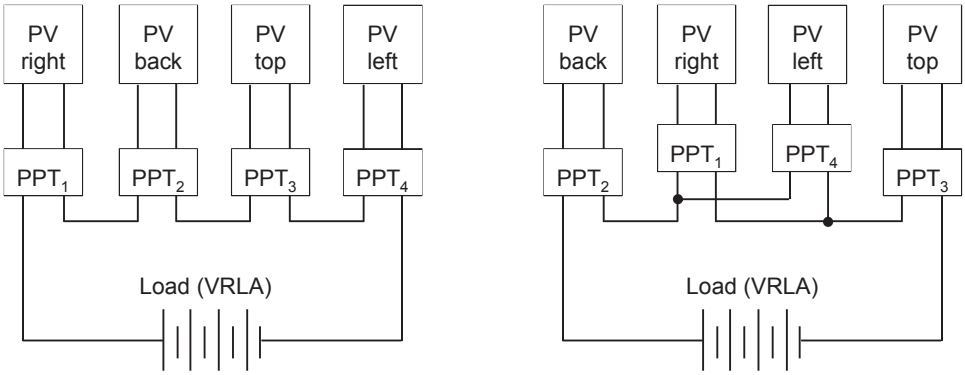


**(a) Series** **(b) Series–Parallel (Left//Right)**

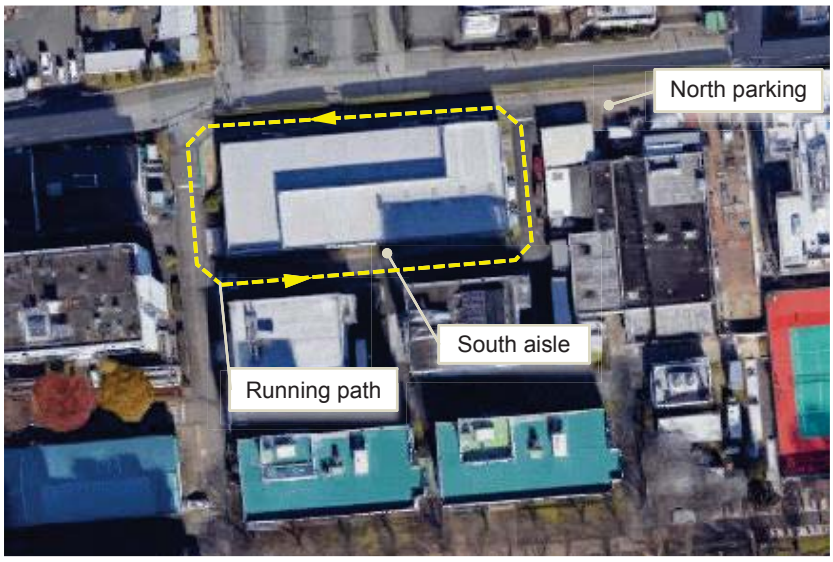


**(c) Experimental location**

**Fig. 6: Different connections of the multiple PPT system**

**Tab. 3: Results of outdoor experiments at the north parking in winter from 10:30 to 15:30. (PPT outputs were limited because of the PV voltage setting)**

| Averaged values | Series PPT system on 9th DEC | Series–Parallel PPT system | |
|---|---|---|---|
| | | Left//Right on 18th DEC | Top//back on 22nd DEC |
| Horizontal irradiance | 377.4 W/m$^2$ | 389.9 W/m$^2$ | 344.3 W/m$^2$ |
| PPT input power from the top PV | 1.00 | 1.00 | 1.00 |
| PPT input power from the left side PV | 0.62 | 0.50 | 0.81 |
| PPT input power from the right side PV | 0.28 | 0.30 | 0.65 |
| PPT input power from the back side PV | 0.62 | 0.69 | 0.37 |
| Output power of the four PV modules | 2.61 | 2.48 | 2.83 |

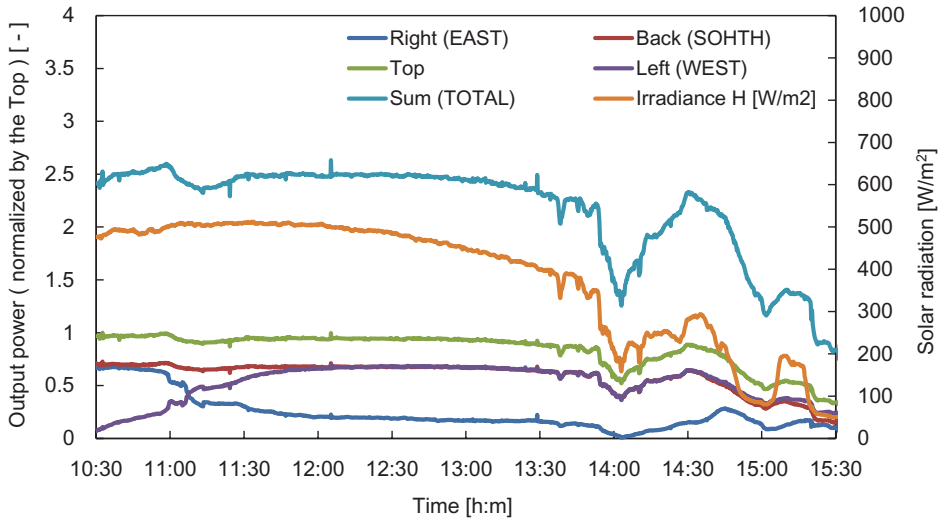


**Fig. 7: Output power of PV modules on Dec 9, 2015 (Series PPT system)**

### *3.2. Battery charging data in summer*

To fix the setting problem mentioned earlier, actual charging was tested for various connections by means of the summer sunlight at the south aisle (Fig. 6). Four valve-regulated lead-acid (VRLA) batteries of 12 V/27 Ah (5 h) were connected to the PPT output as system load. Fig. 8 shows a series PPT system, in which the east PPT underwent the through-mode from the beginning, the west PPT underwent the through-mode at noon. And after 15:00, when the shadows from surrounding buildings appear on the east and south PV, at around 15:30, the overall output power decreases rapidly because of the presence of the shadows of the surrounding buildings. Fig. 9 shows the result of the series–parallel PPT system. The west and east PPTs were connected in parallel; thus, the output currents for both are confluent with those of the top and south PPT. Except after 15:00, no PPTs underwent the through-mode.

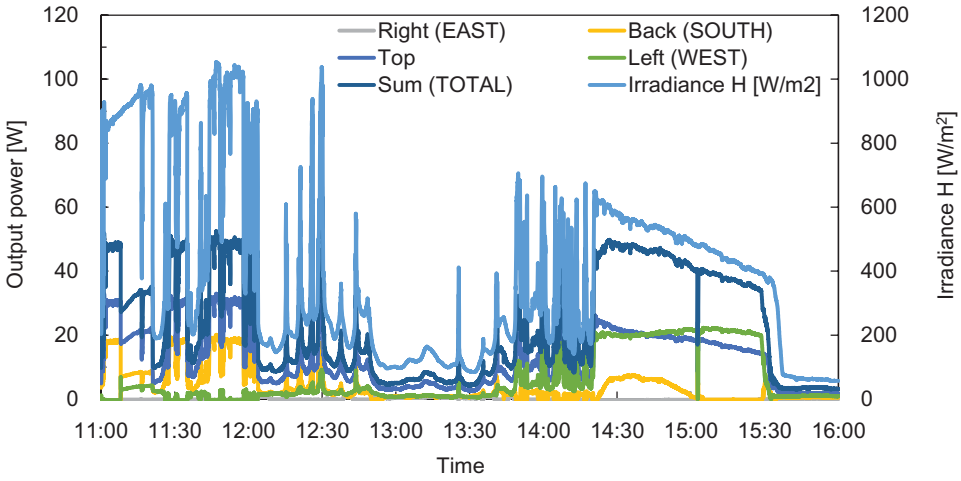


**Fig. 8: Output power of PV on Sep 27, 2016 (four series PPTs for four VRLA systems)**

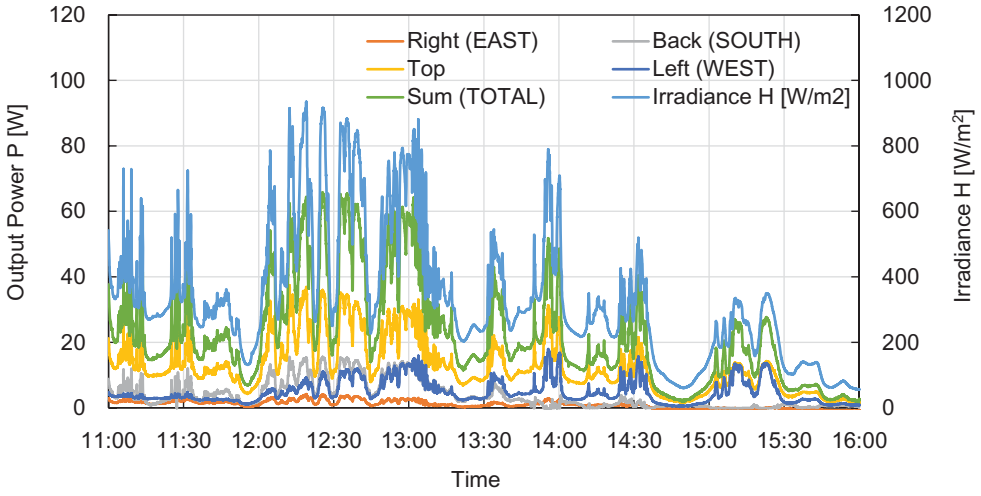


**Fig. 9: Output power of PV modules in Sep 26, 2016 (Series–Parallel PPT system)**

### *3.3. Irradiance on vertical surfaces*

The output power is proportional to the PV current, which is proportional to the irradiance. Therefore, we must determine how to utilize the irradiance on three vertical surfaces. Different azimuth angles of the vertical surface imply an increase in the peak-time difference. In a calculation, it seems easy to add solar irradiance at different angles; however, in an actual system, it is difficult to collect the generated power through simple summation. This is because a low power implies low voltage output of a PPT in a system, and the load voltage is much higher than that of PV modules.

$$P \propto I_{SC} \quad \text{(eq. 1)}$$

$$I_{SC} \propto Irr \quad \text{(eq. 2)}$$

$$E = \sum Irr \quad \text{(eq. 3)}$$

$$k = \frac{E_{Hrzn}}{E_{ESW}} \quad \text{(eq. 4)}$$

where $P$ (W) is the output power of the PV module, $I_{SC}$ (A) is the short-circuit current of the PV module, $Irr$ (W m$^{-2}$) is the solar irradiance onto the PV module, $E$ (W m$^{-2}$) is the summation of the irradiance on different angled surfaces, and $k$ is the imbalance ratio between horizontal irradiance and three vertical surfaces.

Fig. 10 shows the hourly output data of solar irradiance from METPV-11 as a standard meteorological data in Japan released by NEDO/JMA (2016). The figure shows the mean data of a clear day near the university (distance is less than 10 km) in Ebina city, with an irradiance from four directions. Yoshio (2016) recently showed energy utilization in four directions in an architectural study. To utilize a vertical surface efficiently, irradiance on the three walls can be added for collecting PV module's current in the East, South, and West (ESW) directions. As indicated in Fig. 10(b), ESW can function accurately with respect to the horizontal surface. Especially, within few hours before or after noon, the imbalance ratio of irradiance between the horizon and ESW surfaces is less than two.

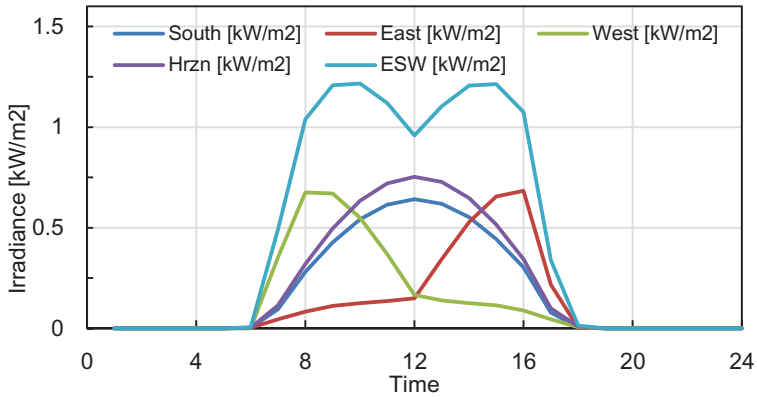


**(a) Irradiance**

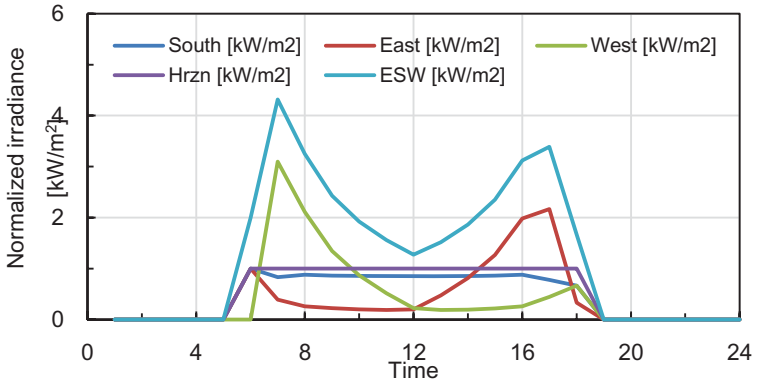


**(b) Normalized Irradiance (Imbalance ratio)**

**Fig. 10: Meteorological data for 25th September in Ebina city (N35°26.0, E139°23.2/METPV)**

When imbalance ratio is smaller, other combination circuitries of the multiple PPT system are also possible (Figs. 11 and 12). PV modules on the three vertical surfaces are connected to a single PPT in parallel. Further, for the PV module on the delivery box's top surface, another PPT is connected to the PPT in series or parallel.

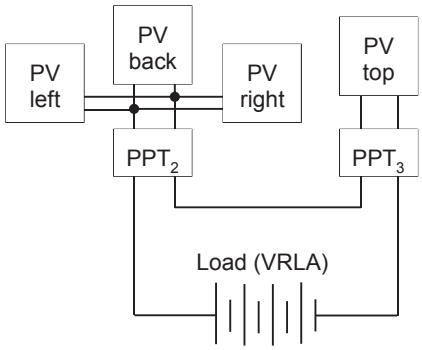


**Fig. 11: Series PPT system for collecting individual current (three vertical PV modules are connected in parallel to one PPT, and another PPT is connected at the top surface)**

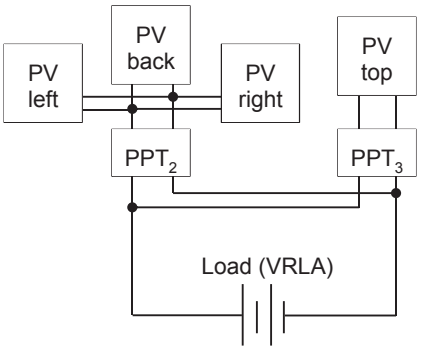


**Fig. 12: Parallel PPT system to collect individual current (three vertical PV modules are connected in parallel to one PPT, and another PPT is connected at the top surface)**

Fig. 13 shows the charging results of a 2-series PPT system on a fine summer day. In the figure, the load comprises four VRLA batteries in series. As shown, the system does not work well even though enough irradiance was present. The PPT output was less than 0.5 A and the boost voltage was imbalanced; thus, the PV modules were unable to operate at the peak power point. The averaged output power was 25.1 W for 5 h. Fig. 14 shows the charging results of a 2-parallel PPT system on a clear summer day; the load comprises four VRLA batteries: two units in series and two units in parallel. As shown, the output power was unstable from 11:00 to 11:10; however, this fluctuation was due to the opening of the back hatch of the delivery box. From 11:10 to 16:10, the PV system of the solar EV generated 51.1 W on an average. It was found that a 180-min

PV charge produces 150 Wh (= 540 kJ) of electrical energy into the load battery even when the irradiance decreased.

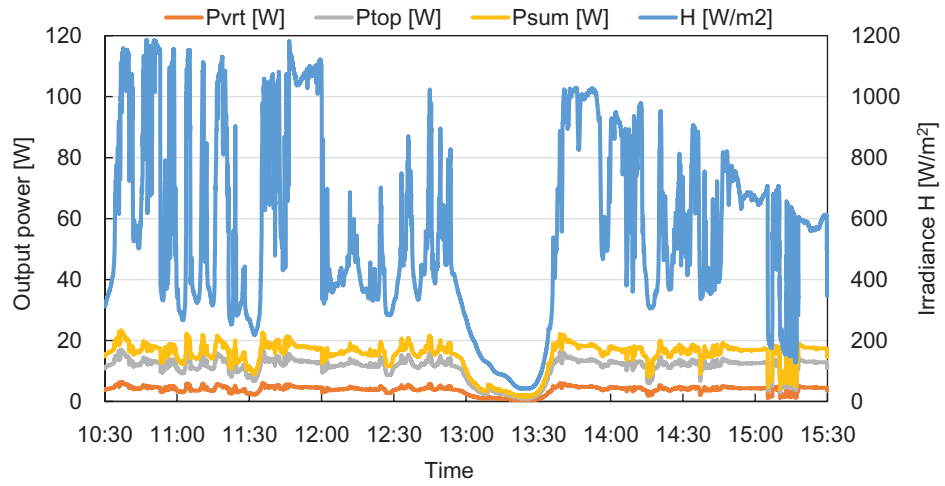


**Fig. 13: Output power of PV on Aug 24, 2016 (2 series PPTs for a 4-series VRLA system)**

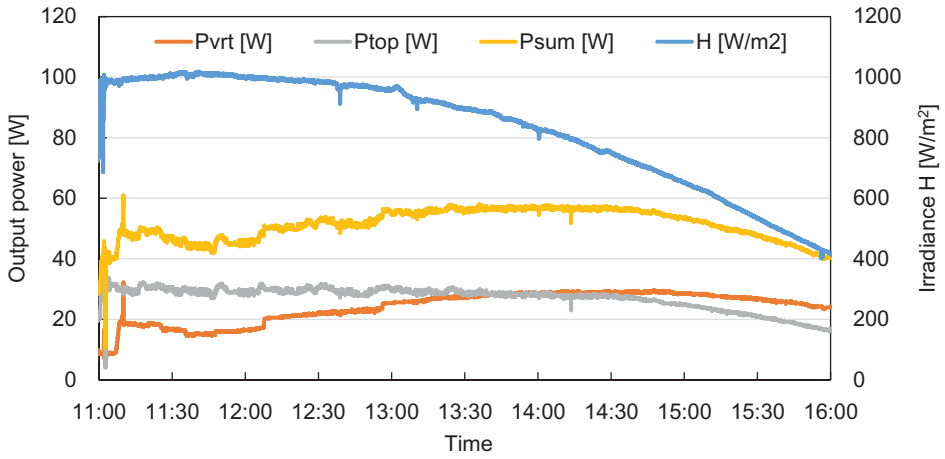


**Fig. 14: Output power of PV on Aug 26, 2016 (2 parallel PPTs for a low voltage VRLA system)**

Table 4 shows the results of the overall experiments at the south aisle in summer; the parallel PPT system showed a slightly better performance. However, the scattering irradiance affects the vertical surfaces, and more data must be collected to discuss an optimum system.

**Tab. 4: Results of outdoor charging experiments of 5 h at the south aisle in summer.**

| PPT System / Average values | Series on 27th Sep | Series–Parallel (left/right) on 26th Sep | Series (top, vertical) on 24th Aug | Parallel (top/vertical) on 26th Aug |
|---|---|---|---|---|
| Horizontal irradiance | 389.6 W/m$^2$ | 332.7 W/m$^2$ | 560.1 W/m$^2$ | 811.5 W/m$^2$ |
| Charged Power | 23.7 W | 22.1 W | 25.1 W | 51.1 W |
| *P*/*H* | 6.1% | 6.6% | 4.5% | 6.3% |
| | (Scattering irradiance effect ) | | | (Low voltage load) |

### *3.4. Running experiment*

Power and energy consumptions of the solar EV were measured through an experiment by using a 5 kg Li-ion rechargeable battery. Fig. 15 shows the measurement result of the scooter riding around a building on a flat asphalt road in winter. As indicated in the figure, the top speed reached 25.1 km/h and the peak current was 30 A, approximately. In addition, the average power consumption was 1.09 kW. This result shows that the solar-

energy-charging time would be at least 20 times longer than running time in fine weather.

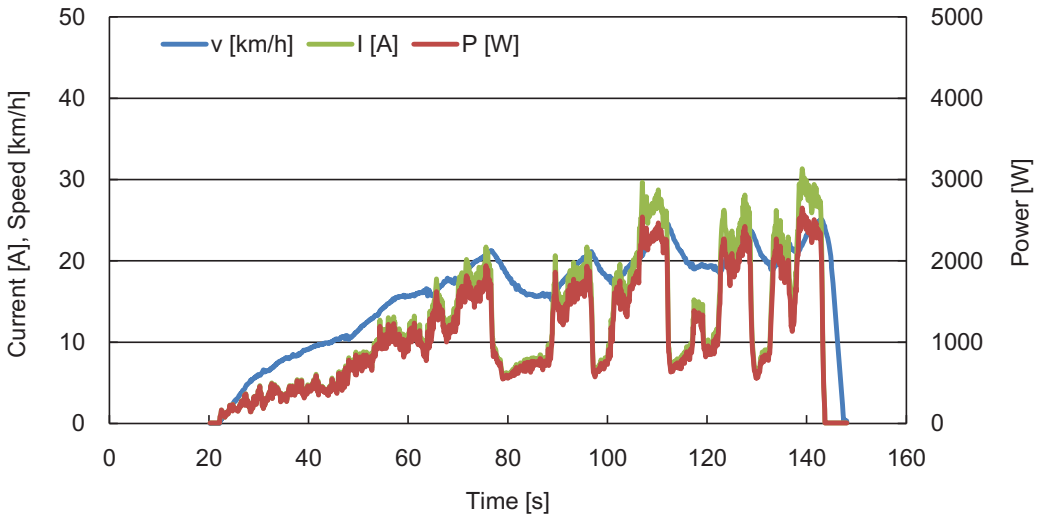


**Fig.15: Test data of travelling 0–25 km/h around the building (Feb 18, 2016).**

## 4. Conclusions

In this paper, we discussed about the solar EV converted from the three wheel scooter Honda Gyro Canopy widely used for delivery service in Japan. The limited data of outdoor experiments showed that the series–parallel PPT system produced more energy than the series or parallel PPT systems at the south aisle in summer. There is more room to discuss the optimization of a multiple PPT system. However, we must also consider the system load voltage of the VRLA battery and the effect of scattering irradiance. Experiments were conducted in which the solar EV was driven with the help of a 5 kg Li-ion rechargeable battery around a building on a flat asphalt road. The result showed that the average power consumption was 1.06 kW at an average speed of 15.9 km/h (the peak speed was 25.1 km/h), electric energy consumption ratio was 15 km/kWh.

In photovoltaic and automotive industry, 100 thousand delivery boxes with PV system for the Solar EVs means creating at least 10 MW new PV business market. With amount of 100 thousand Solar EV utilizing solar energy, if the ratio of charging time / running time was 3-4, 15-20 thousand Solar EVs are equivalent to zero energy vehicle (ZEV).

### *4.1. Remaining Problems*

- For the PPT, both optimum connection and protective limit settings must be discussed.
- Optimum PPT control at the running state must be discussed. (Direction of sunlight and shading area will be variable.)
- The installation area of the PV modules, such as the rooftop and front fairing, must be increased.
- The vehicle's weight must be reduced, and the rolling resistance of the tires and air flow drag should be improved.
- The delivery box needs an advertisement area, and strong reflective sunlight due to the PV modules must be avoided for the benefit of other drivers.
- The merits for bifacial PV cells should be investigated.

## 5. References

bSolar Ltd, 2012. Electrical Characteristics, BSBF-18.5/22 Bifacial Monocrystalline Silicon Solar Cell, p. 2.

ST Microelectronics, 2012. Interleaved DC-DC boost converter with built-in MPPT algorithm, Doc ID 17588 Rev 4.

Takanori Matsuyama, Kazuhiro Igura, Hiroshi Fukukita et al., 2014. Experiment Introduction of Distributed Maximum Power Point Tracking Systems for PV System and Effect Applied to Solar Car, J. JSES, Vol. 40, No. 4, 51–60.

Yoshio Hashimoto, 2016. Aqua Innovation International Center at Shinshu University, J. IEIE Jpn. Vol. 36, No. 8, 37–40.

Youhei Takigawa, Tomoki Kinno, Kazuto Yukita et al., 2013, A Distributed MPPT introduction evaluation of solar power, Proc. JSES/JWEA Joint Conf., Vol. 100, 369–372.

*Web:*

HONDA GYRO, 2015, https://ja.wikipedia.org/wiki/%E3%83%9B%E3%83%B3%E3%83%80%E3%83%BB%E3%82%B8%E3%83%A3%E3%82%A4%E3%83%AD.

JMA, 2016. METPV-11, NEDO, http://app0.infoc.nedo.go.jp/